Microstructural Evolution and Solidification Behavior of Al-Mg-Si Alloy in High-Pressure Die Casting

SHOUXUN JI, YUN WANG, D. WATSON, and Z. FAN

Microstructural evolution and solidification behavior of Al-5 wt pct Mg-1.5 wt pct Si-0.6 wt pct Mn-0.2 wt pct Ti alloy have been investigated using high-pressure die casting. Solidification commences with the formation of primary α-Al phase in the shot sleeve and is completed in the die cavity. The average size of dendrites and fragmented dendrites of the primary α-Al phase formed in the shot sleeve is 43 μm, and the globular primary α-Al grains formed inside the die cavity is at a size of 7.5 μm. Solidification inside the die cavity also forms the lamellar Al-Mg_2Si eutectic phase and the Fe-rich intermetallics. The size of the eutectic cells is about 10 μm, in which the lamellar α-Al phase is 0.41 μm thick. The Fe-rich intermetallic compound exhibits a compact morphology and is less than 2 μm with a composition of 1.62 at. pct Si, 3.94 at. pct Fe, and 2.31 at. pct Mn. A solute-enriched circular band is always observed parallel to the surface of the casting. The band zone separates the outer skin region from the central region of the casting. The solute concentration is consistent in the skin region and shows a general drop toward the center inside the band for Mg and Si. The peak of the solute enrichment in the band zone is much higher than the nominal composition of the alloy. The die casting exhibits a combination of brittle and ductile fracture. There is no significant difference on the fracture morphology in the three regions. The band zone is not significantly detrimental in terms of the fracture mechanism in the die casting. Calculations using the Mullins and Sekerka stability criterion reveal that the solidification of the primary α-Al phase inside the die cavity has been completed before the spherical α-Al globules begin to lose their stability, but the α-Al grains formed in the shot sleeve exceed the limit of spherical growth and therefore exhibit a dendritic morphology.

DOI: 10.1007/s11661-013-1663-5

I. INTRODUCTION

HIGH-PRESSURE die casting (HPDC) is one of the most popular manufacturing processes used in the casting industry. The attractiveness of HPDC is its ability to make near net-shape parts with tight tolerances, requiring little or no machining.[1,2] HPDC castings often have low ductility and are used for nonstructural applications. However, they have been attracting increased interest in the products of structural applications, particularly in transportation such as automotive markets because of the driving force in terms of weight savings leading to improved fuel economy.[3,4] An extensive range of aluminum HPDC parts are used in the automotive industry, which include transmission housings, cylinder heads, inlet manifolds, engine sumps, brackets, heat sinks, stators, as well as for decorative trim items.[5,6] Moreover, an increasing trend in replacing steel parts with the lighter aluminum parts has seen aluminum HPDC parts being used extensively in other automotive areas. One of the significant developments in recent years has been their application in aluminum car body structures.[3,7,8] Unique mechanical properties are required for this specific application. For example, the ductility of aluminum components for car body structures requires thin wall die castings with at least 15 pct of elongation. To achieve the required elongation, several critical aspects need to be precisely controlled during manufacturing which include an optimized alloy composition, low level of gas and impurities in melt before solidification, minimized defect levels, and an optimized microstructure in the castings. These are associated partially or completely with the solidification of the castings.

It has been found that Al-Mg-Si-based alloys are capable of providing high ductility and an excellent combination of mechanical properties for die castings in the as-cast state.[9] However, the diecast Al-Mg (-Si)-based alloys are known to have high solidification shrinkage which, therefore, increases the difficulty of producing castings with high integrity.[10,11] As such, the microstructural evolution and the related control during solidification are becoming very important for achieving enhanced mechanical properties of the Al-Mg-Si alloy.

The solidification of Al-Mg (-Si)-based alloys has been the subject of many studies, but most of them fall into the category of wrought alloys[12,13] or high silicon (>5 wt pct Si) and low magnesium (<1 wt pct) cast alloys (*e.g.*, A356)[14,15] produced by sand casting or gravity die-casting

SHOUXUN JI, Lecturer, YUN WANG, Senior Research Fellow, and Z. FAN, Professor, are with the Brunel Centre for Advanced Solidification Technology (BCAST), Brunel University, Uxbridge UB8 3PH, UK. Contact e-mail: shouxun.ji@brunel.ac.uk D. WATSON, Ph.D. Student, is with the Brunel Centre for Advanced Solidification Technology (BCAST), Brunel University, and also with the Jaguar Cars Limited, Engineering Centre, Abbey Road, Coventry CV3 4LF, UK.

Manuscript submitted April 25, 2012.
Article published online February 16, 2013

process. Previous studies were rather limited in describing the solidification and microstructural evolution of high magnesium (>4 wt pct) and silicon (>1.5 wt pct) cast alloys in HPDC process. Otarawanna *et al.*[16] studied the microstructural formation of AlSi4MgMn and AlMg5Si2Mn castings and found that the salient as-cast microstructural features were similar for both alloys in terms of the externally solidified crystals, defect bands, surface layer, grain size and distribution, porosity, and hot tears. Jie *et al.*[17] investigated the microstructure of Al-21.6 wt pct Mg alloy solidified under high pressure inside a cylindrical container at a pressure up to 2 GPa. They found that the amount of β-Al_3Mg_2 phase decreased with the increasing pressure, and a supersaturated Al(Mg) solid solution was formed at 2 GPa. Kimura *et al.*[18] studied the effect of grain refiner and grain size on the cracking susceptibility of Al-4.5 wt pct Mg diecast alloy. They found that the addition of 0.08 wt pct Ti and 0.016 wt pct B could achieve significant grain refinement and, therefore, it suppressed cracking formation in Al-Mg die castings. Recently, the authors investigated the effect of main alloying elements on the mechanical properties of Al-Mg-Si diecast alloy and optimized the composition and casting process to satisfy the requirement of strength and ductility.[9] In HPDC process, the melt is injected into the die cavity under high speed (30 through 50 m/s ingate velocity for aluminum alloys), and solidified under high pressure (up to 200 MPa in the die cavity) and high cooling rate (up to 10^3 K/s).[19] This results in unique solidification behavior and offers a fundamental difference to other casting processes. Therefore, theoretical understanding of the solidification process and microstructural evolution in HPDC is important for improving the process itself, microstructural control, and the mechanical properties. Moreover, defect formation is closely related to the solidification and microstructure of the castings. This is particularly important in determining the mechanical properties of ductile diecast aluminum alloys.

In the current study, investigation of the solidification process and microstructural evolution of ductile aluminum alloy has been carried out using HPDC process. The solidification behavior in the shot sleeve and in the die cavity was examined for the formation of the primary α-Al phase, eutectic phase, and Fe-rich intermetallics in Al-5 wt pct Mg-1.5 wt pct Si-0.6 wt pct Mn-0.2 wt pct Ti (abbreviated as AlMgSi hereafter) alloy.[9] The morphology, size, and size distribution of the primary α-Al phase were characterized under different solidification conditions. The phases formed in the different stages of solidification were identified and quantified. In the discussion, the growth morphology of the primary α-Al phase formed in the shot sleeve and in the die cavity was analyzed using the Mullins–Sekerka instability theory. Jackson–Hunt theory was also used to calculate the growth rate of Al-Mg_2Si eutectic phase during solidification.

II. EXPERIMENTAL

Commercial grade ingots of pure aluminum, pure magnesium, Al-15 wt pct Si, Al-20 wt pct Mn, and Al-10 wt pct Ti master alloys were used as base materials. Each of them was supplied at a specified composition with known industrial purity. During experiments, each element was weighed to a specified ratio with an allowance for burning loss during melting. Batches of 6 through 10 kg were melted in a clay–graphite crucible using an electric resistance furnace at 1003 K (730 °C). The melt was thoroughly stirred to ensure complete dissolution and homogenization. For all the experiments, the melt was subjected to fluxing and degassing using commercially available fluxes and N_2. The N_2 degassing lasted 3 minutes with a granular flux covering the surface of the melt. Then, the melt was held at 973 K (700 °C) for 20 minutes before taking a sample for composition measurement.

A $\phi 40 \times 60$mm cylindrical casting was made in a steel mould for composition analysis. The cylindrical casting was cut across the diameter at 15 mm from the bottom and ground to 800 grit. The composition measurements were conducted with an optical mass spectrometer, in which five spark analyses were performed, and the average value was taken as the actual chemical composition of the alloy.

After compositional analysis and skimming, the melt was manually dosed and subsequently released into the shot sleeve of a 2800-kN cold chamber HPDC machine for casting under an optimized casting condition. The temperature of the die block was controlled at 484 K (211 °C) and the temperature of shot sleeve was controlled at 423 K (150 °C) during casting. The pouring temperature of the melt was 923 K ± 5 K (650 ± 5 °C) measured by a K-type thermocouple. The diecast samples for tensile tests were schematically shown in Figure 1, which were designed according to the specification defined in ASTM B557-06.

The samples for microstructural evaluation were taken from the middle of the tensile test bar, and examined using a Zeiss optical microscope (OM) with quantitative metallography. All metallographic samples were prepared by a standard technique. The grain size, volume fraction, and the shape factor of the solid phase were measured using an AxioVision 4.3 Quantimet digital image analysis system. Five different fields of view were analyzed from each specimen, and the average was taken as the actual measurement value. Scanning electron microscopy (SEM) analysis was carried out with a field emission gun Zeiss SUPRA 35VP machine, equipped with an energy dispersive spectroscopy (EDS) facility and operated at an accelerating voltage ranging from 3 to 20 kV. The quantitative EDS results were obtained under a 20-kV accelerating voltage with the system being calibrated before each session. The accuracy of the quantitative EDS was within 0.1 pct. To minimize the influence of the interaction volume, at least five analyses on selected grains were conducted for each phase and the average was taken as the measurement.

III. RESULTS

A. *Mechanical Properties and Microstructure of the Die Castings*

Our extensive measurement of the diecast AlMgSi alloy have confirmed that the yield strength is at a level of 150 MPa, the ultimate tensile strength is at a level of

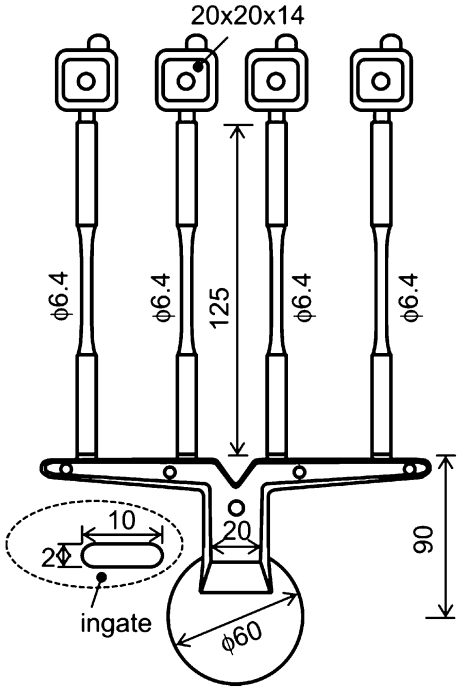

Fig. 1—Schematic diagram of diecast specimens for standard tensile testing according to the specification defined in ASTM B557-06. The overflow and biscuit are designed in association with a 2800-kN cold chamber die-casting machine (All dimensions are given in mm).

300 MPa, and the elongation is at a level of 15 pct.[9] Clearly, the alloy shows high ductility, in comparison with the alloys currently available in industry. This ductility is important for the joining of thin wall castings to other components by riveting. Although the mechanical properties of the alloy depend on several factors related to alloy chemistry and manufacturing process, microstructural evolution during solidification is one of the most important aspects for achieving high ductility.

Figure 2 shows the microstructures of the cross section of a tensile specimen in the diecast AlMgSi alloy. It shows a solute-enriched circular band that is parallel to the surface of the casting. The similar phenomenon of band formation has been observed by Dahle *et al*. for different alloys.[16,20] The band separates the outer skin and the central region of the casting. Two types of primary α-Al phases are seen in the microstructure shown in Figure 2. The primary α-Al phase that solidifies in the shot sleeve exhibits a relatively large size with dendritic or fragmented dendritic morphology. The primary α-Al phase that solidifies in the die cavity shows a relatively smaller size with a globular morphology. A higher volume fraction of the primary α-Al phase that solidifies in the shot sleeve is observed in the central region compared with the outer skin region of the casting, as shown in Figures 2(b) to (d). The outer skin thickness was measured at 1.0 mm for the AlMgSi alloy in this study, which is smaller than the thickness of 1.5 mm measured in Al-Si-Cu alloys.[16] In the transition band zone, the volume fraction of eutectic phase is higher compared with both the skin and the central region.

The composition profile shown in Figure 3 is an example of the variation in magnesium and silicon concentration from the surface to the center of the AlMgSi casting. The concentrations are consistent in the skin region with a general drop toward the center inside the band. For instance, the Mg concentration is close to the nominal composition of 5 wt pct in the skin region and gradually decreases to 3.8 wt pct at the center of the casting, whilst the Si concentration is also close to its nominal composition at 1.5 wt pct in the skin region but slightly lower in the central region. The band zone is found to be enriched in Mg and Si to 8.8 wt pct and 2.9 wt pct, respectively. The peak of the solute enrichment in the band zone is much higher than the nominal composition in the alloy. The results confirm the segregation of the solute distribution on the cross section of the die castings. The drop in the solute content of Mg and Si from the surface to the center as well as the peak in the band zone is unusual for conventional solidification. According to the phase diagram and Scheil equation, the composition profile would predict the solute content to increase from the surface to the center of the casting if the solidification front progresses from the surface to the center. The formation of central core is related to the solidification conditions and, consequently, has a very different history. However, the relative movement of melt at different parts is one of the most important reasons to form band zone during solidification.[16,20] One can speculate that the outer region is a chill zone, and the central is ''backfill'' from the runner during solidification to vary the microstructure.

In order to assess the effect of the nonuniform solute distribution on the mechanical properties of the die castings, a sample was sectioned perpendicularly to its fracture surface. Figure 4 shows the microstructure along the fractured surface in the skin region, band zone and central region. It is seen that the sample is uniformly elongated and no apparent neck is observed around the fractured surface. The primary α-Al grains are stretched toward the fractured surface. The micrographs in Figure 4 confirm that the fracture occurs mainly along the α-Al grain boundaries, and the fracture across the primary α-Al grains is also found in the skin region, band zone and central region. Meanwhile, a few subsurface pores in irregular shapes are observed close to the fractured surface in the band zone and the central region. This suggests that the cracking as the fracture source is likely initiated in the band zone and the central region under stress. The cross-sectional micrographs in Figure 4 also show that the fracture is a combination of grain–boundary separation and the cleavage fracture across primary α-Al grains. To confirm the detail, SEM fractographs of a sample fractured at an elongation of 18.4 pct with ultimate tensile strength of 302.5 MPa are shown in Figure 5. In the fractographs, porosities are seen as the main defects in the die castings. The fractograph in Figure 5(a) shows that the fracture is relatively flat in the skin region, but coarse and uneven in the central region. The transition occurs in the band zone. However, there is no significant difference on the fracture morphology in the three regions. A large

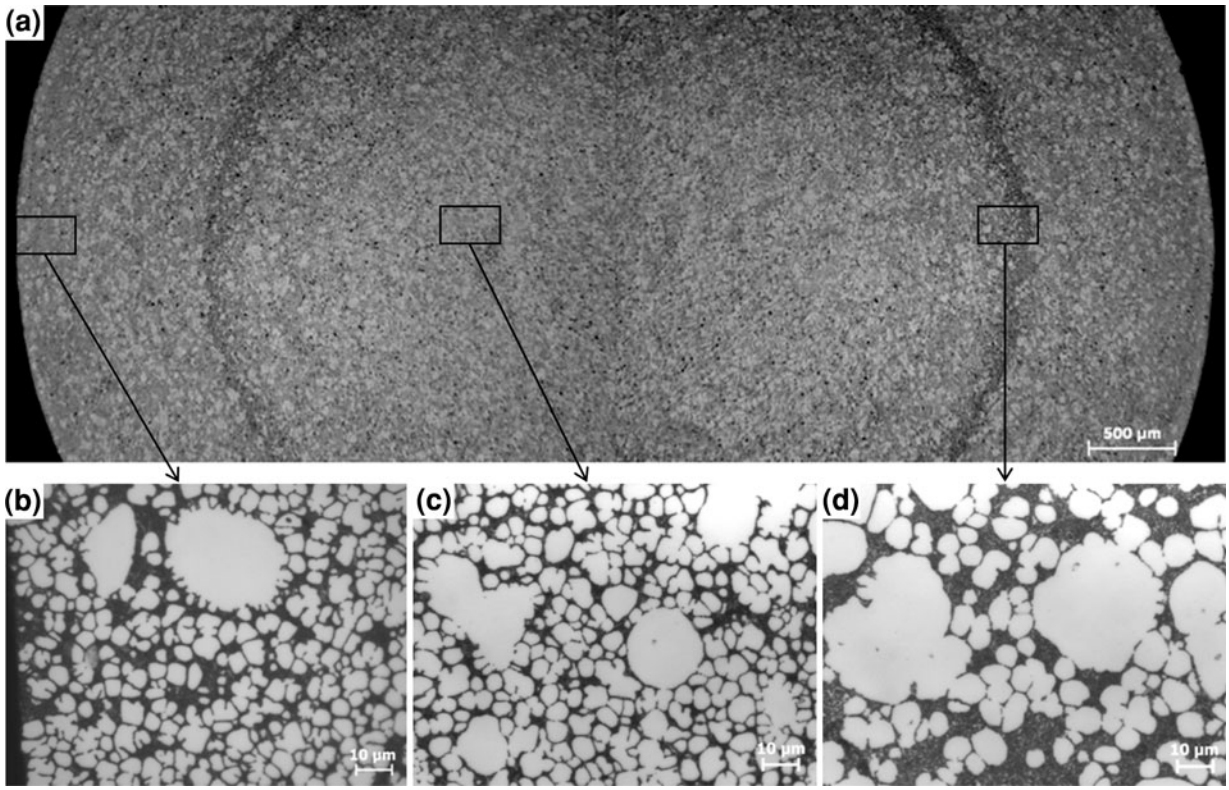

Fig. 2—Optical micrographs showing the microstructure of the diecast Al-5 wt pct Mg-1.5 wt pct Si-0.6 wt pct Mn-0.2 wt pct Ti alloy, (*a*) on a cross section of ϕ6.4-mm tensile test specimen, (*b*) in the outer skin region, (*c*) in the central region, and (*d*) in the band zone. The circular segregation band is 1 mm from the surface of casting and has a width from 100 to 150 μm.

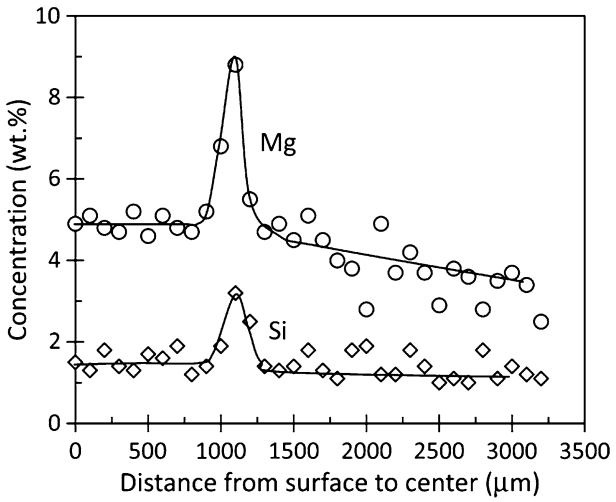

Fig. 3—SEM/EDS analysis showing the concentration profile of Mg and Si on a section of diecast ϕ6.4mm tensile specimen of the Al-5 wt pct Mg-1.5 wt pct Si-0.6 wt pct Mn-0.2 wt pct Ti alloy.

proportion of intergranular fracture around the fine primary α-Al grains, the cleavage fracture in the relatively large primary α-Al grains, and the decohesion between the Mg_2Si phase and Al phase in the eutectic are observed as the main fracture mechanism in the three regions. The difference in the central region is that small dimpled rupture is also observed in the region. Therefore, the die casting of ductile AlMgSi alloy exhibits a combination of brittle and ductile fracture. Although the solute-rich segregation in the band zone could initiate the cracking for fracture, the similar cracking is also found in the central region. Therefore, the band zone is not significantly detrimental in terms of the fracture mechanism in the diecast AlMgSi alloy.

B. *The Primary Phase Formed in the Shot Sleeve and in the Die Cavity*

Figures 6 and 7 show the microstructures of the diecast AlMgSi alloy with different amounts and morphology of the primary α-Al phase. Two types of primary α-Al phase are seen in the matrix. One shows the morphology of dendrites or fragmented dendrites with a larger size (denoted as α_1), and the other is fine globules (denoted as α_2). During die casting, the solidification commences when the melt is poured into the shot sleeve. Because the cooling rate inside the shot sleeve is similar to that in gravity die casting, a cooling rate ranging from 20 to 80 K/s could be achieved,[19] with the solidification initiating from the nucleation of the α-Al crystals that subsequently grow dendritically in the shot sleeve. The primary α-Al dendrites are fragmented when the melt is injected into the die cavity through the ingate at a high speed, resulting in the formation of fragmented dendrites in the microstructure. Figures 6 and 7 also show the different amounts of the primary α-Al crystals solidified in the shot sleeve, which is determined by the pouring temperature, the rest

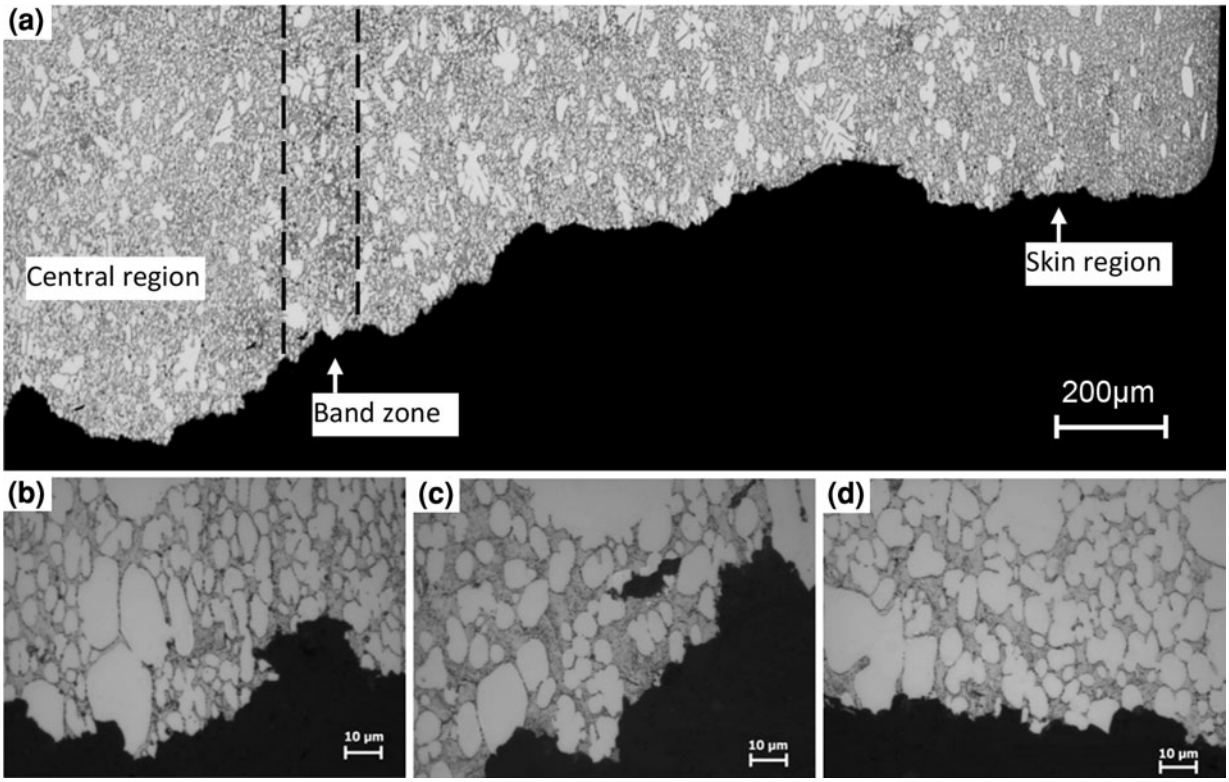

Fig. 4—Optical micrographs showing the microstructure on a section perpendicular to the fractured surface of the AlMgSi alloy, (*a*) over all microstructure, (*b*) the skin region, (*c*) the band zone, and (*d*) the central region.

time, and the temperature of the shot sleeve. Figure 8 shows the size distribution of the primary α-Al phase solidified in the shot sleeve, in which the grain size is between 15 and 100 μm with a mean of 43 μm. The distribution of the primary α-Al phase shows a very close match to a Gaussian distribution, suggesting that the solidification in the die-casting process is relatively consistent for the different amounts of primary α-Al phase.

When the melt is injected into the die cavity, the remnant liquid in the mixture that contains α_1 phase starts to solidify immediately. As shown in Figures 6(b) and 7(b), α_2 phase shows a similar globular morphology, although the amount is at different levels. This suggests that spherical or globular growth occurs during the solidification inside the die cavity. The size distribution of α_2 is shown in Figure 9, in which the grain size is between 3 and 12 μm and the average is 7.5 μm. The distribution curve also matches a Gaussian distribution with a mean of 7.5. As the solidification inside the die cavity occurs under a high cooling rate, which is typically ranging from 400 to 500 K/s,[19] the high cooling rate increases the nucleation rate, and thus stable globular growth could occur for α_2 (to be analyzed in greater detail in Section IV).

Figure 10 shows the relationship between the solid fractions of α_1 and α_2. For the given alloy, the amount of the primary α-Al phase is mainly determined by the composition. This means that the amount of $\alpha_1 + \alpha_2$ is the same for a given composition, although the solidification could be divided into several stages. Therefore, as shown in Figure 10, the increase in the amount of α_1 results in a decrease in the amount of α_2. Figure 11 shows the mean grain size and the shape factor for the primary α_1 and α_2 aluminum phase. For α_1, the mean grain size slightly increases and the shape factor slightly decreases with the increase of the volume fraction of α_1. This indicates that the dendritic growth is enhanced at the higher volume fraction of α_1 in the shot sleeve. Therefore, the control of the solidification in the shot sleeve is critical to optimize the microstructure. On the other hand, the mean grain size and the shape factor of α_2 are essentially the same regardless of the volume fraction. The mean grain size is at a level of 7.5 μm, and the shape factor is 0.75.

SEM observation of an etched sample was carried out to assess the morphology of the primary α-Al phase solidified inside the die cavity. As shown in Figure 12, the boundaries of the fine primary α-Al phase are clear. This implies that many of the globular α-Al phase formed in the die cavity are likely to be individual ones. The solidification of each globule could be initiated from an individual nuclei and grow independently. To further confirm the solidification behavior, quantitative EDS analysis was performed on the different samples. Figure 13 gives the SEM/EDS results of the solid solubility of Mg and Si in both α_1 and α_2 primary phases as a function of the distance from the grain edge. The average Mg concentrations are 4.48 ± 0.22 and 4.52 ± 0.19 wt pct for α_1 and α_2, respectively. Although it is statistically overlapped, the slightly higher average of Mg concentration in the fine α_2 grains reflects the enrichment of the solute element in the

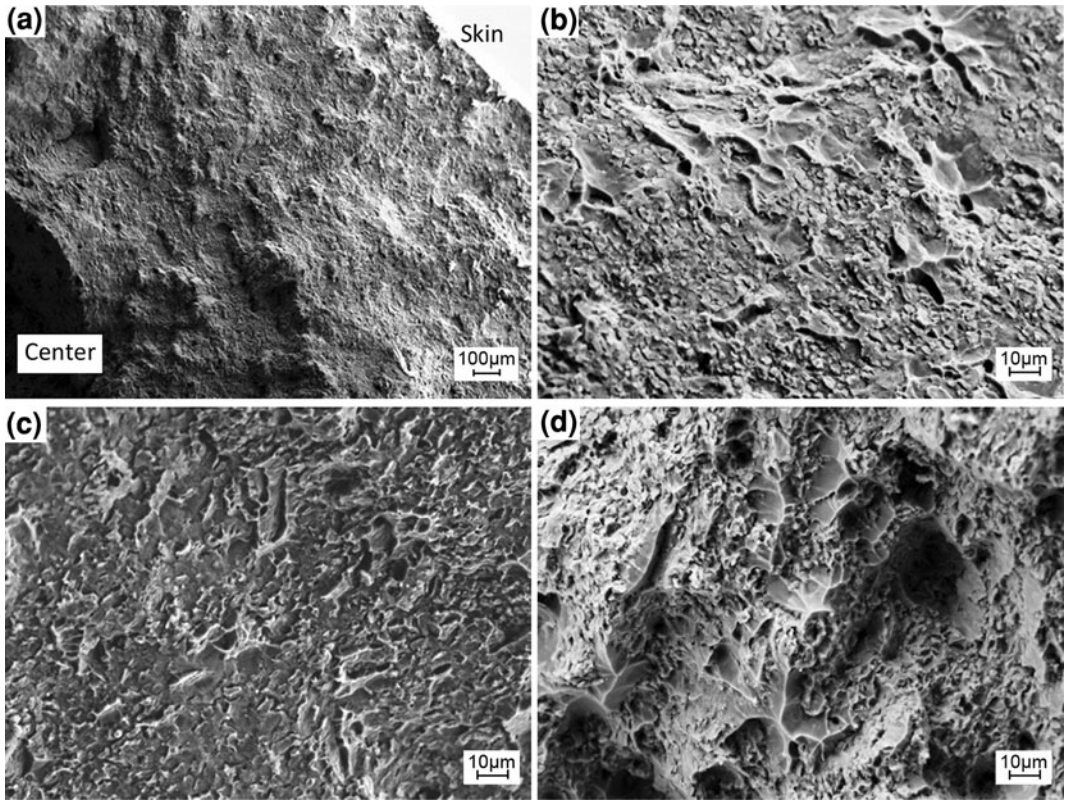

Fig. 5—SEM images of the fractured surface of the AlMgSi alloy, (*a*) overall fractograph from the skin to the center of the tensile test bar, (*b*) the fractograph of the skin region, (*c*) the fractograph of the band zone, and (*d*) the fractograph of the central region.

remnant liquid inside the die cavity. In addition, according to the equilibrium Al-Mg-Si phase diagram,[21] the lower solidification temperature for the remnant liquid would result in a higher Mg content in the α_2 solid solution phase. Meanwhile, the concentration of Si (0.53 ± 0.09 wt pct) in α_1 and α_2 aluminum phase does not show much variation. One important feature in the EDS analysis shown in Figure 13 is that there is hardly any Mg and Si content gradient across α_1 and α_2 aluminum phase. It is worth emphasizing that the concentration variation across the tensile sample, as shown in Figure 3, is a phenomenon of macrosegregation that is related to the mould-filling process, but the concentration profile in Figure 13 is for individual primary α-Al grain regardless of the position in the sample.

C. *Eutectic Phase*

The morphology of the eutectic phase is shown in Figure 14. EDS analysis confirms that the lamellar microstructure of the eutectic consists of α-Al phase and Mg_2Si phase. The size of the eutectic cells is about 10 μm, in which the lamellar α-Al phase is 0.41 μm in thickness. SEM observation on a deep-etched sample reveals that the eutectic Mg_2Si phase exhibits fine lamellae morphology, and branching of the flakes is frequently observed. This suggests that the solidification follows a conventional path under a high cooling rate. There is no thick platelet Mg_2Si phase observed in the samples. The amount of eutectic largely depends on the composition of the alloy. An increased level of Mg and Si in the alloy creates more eutectic phase, which would cause an increase in strength and a decrease in ductility.

D. *Intermetallics*

In the AlMgSi alloy, Mn is kept at a level of 0.6 wt pct, and the Fe is controlled below 0.25 wt pct. Figure 15a shows the intermetallic phase in the matrix (bright phase). The intermetallics exhibit a compact morphology with the size being smaller than 2 μm and are located on the boundary between the primary α-Al grains or between the eutectic cells and the primary α-Al grains. This suggests that the intermetallics are formed in the die cavity, rather than in the shot sleeve. The EDS analysis shown in Figure 15(b) reveals that the compact intermetallic compounds consist of Al, Mn, Fe, and Si with the composition being quantified to be 1.62 at. pct Si, 3.94 at. pct Fe, and 2.31 at. pct Mn, most likely the α-AlFeMnSi, rather than the β-AlFeSi phase.

IV. DISCUSSION

A. *The Growth of Primary α-Al Phase Solidified in the Shot Sleeve (α_1) and in the Die Cavity (α_2)*

Solidification in HPDC process commences when the melt is poured into the shot sleeve.Owing to the relatively low temperature of the shot sleeve, the melt in contact with the shot sleeve is immediately cooled below its liquidus temperature. Heterogeneous nucle-

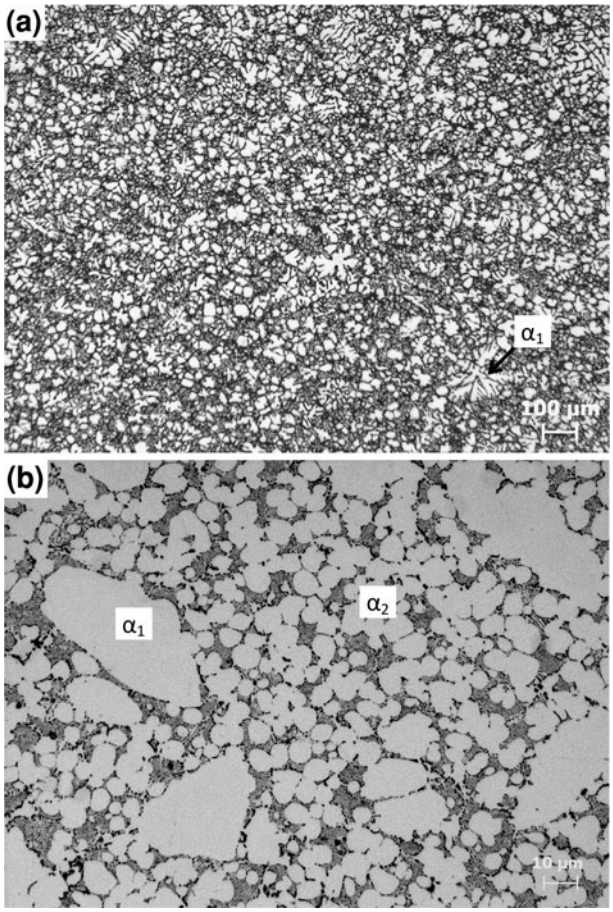

Fig. 6—Microstructures of diecast Al-5 wt pct Mg-1.5 wt pct Si-0.6 wt pct Mn-0.2 wt pct Ti alloy with a primary α_1-Al phase of f_s = 19 pct, (*a*) low magnification image showing the distribution of the primary α_1-Al phase, and (*b*) high magnification image showing details of the morphology of the primary α_2-Al phase solidified within the die cavity.

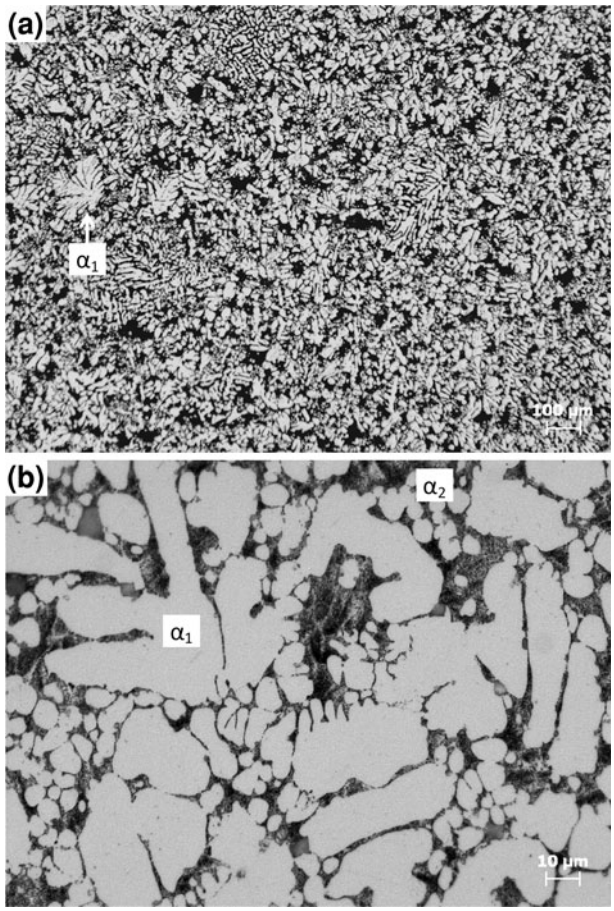

Fig. 7—Microstructures of diecast Al-5 wt pct Mg-1.5 wt pct Si-0.6 wt pct Mn-0.2 wt pct Ti alloy with a primary α_1-Al phase of f_s = 32 pct, (*a*) low magnification image showing the distribution of the primary α_1-Al phase, and (*b*) high magnification image showing details of the morphology of the primary α_2-Al phase solidified within the die cavity.

ation occurs in the melt and grows to form α-Al dendrites (α_1). The dendrites are then partially fragmented while passing the narrow ingate with high speed and turbulent flow during the die-filling process. Because of the temperature variation and high flow rate during die filling, the Stoke's motion in the gravity field and Marangoni motion in the nonuniform temperature field promote the solidified primary phase α_1 to segregate into the middle of casting section, which leads to the formation of nonuniform microstructure in as-cast condition.[22] Marangoni motion is proportional to the temperature gradient, and therefore it is determined by the melt temperature and the die temperature. Stoke's motion is proportional to the square of particle size and reversely proportional to the viscosity of the liquid matrix. Therefore, Stoke's motion becomes significant for large particles and in a liquid with low viscosity.

On the other hand, the high turbulent flow promotes the temperature uniformity in the melt throughout the die cavity. With a high cooling rate provided by the metallic die block, nucleation inside the die cavity is expected to take place throughout the entire volume of the remaining liquid. The numerous nuclei compete growing until solidification finishes under high cooling rate inside the die cavity. The primary α-Al grains formed inside the die cavity (α_2) have been observed to be 7.5 μm in size, indicating that the fine primary α-Al grains could still be within a spherical growth morphology because the dendritic morphology that is established through unstable growth may have not yet developed. This can be explained by applying the Mullins–Sekerka growth theory.[23]

The Mullins and Sekerka growth theory calculates the point where the spherical shape of crystal growing from a melt becomes morphologically unstable when its size exceeds a critical value R_c (in μm)[23]:

$$R_c = \frac{2\Gamma_T(7+4k_s/k_l)}{(T_m - T_\infty)/T_m} = \frac{2(\gamma_{SL}/L_v)(7+4k_s/k_l)}{\Delta T/T_m} \quad [1]$$

where T_m and T_∞ are the melting point and melt temperature, respectively; k_s and k_l are thermal conductivities of liquid and solid Al at the melting point temperature, respectively; γ_{SL} is the interfacial energy at the S/L interface;, and L_v is the latent heat of fusion per unit volume of the solid.

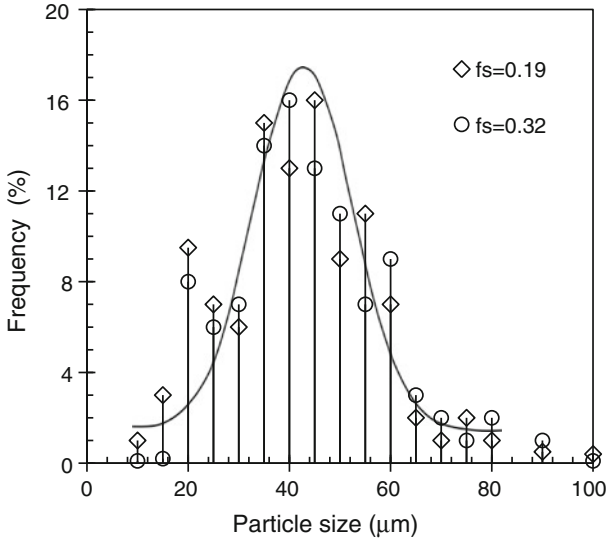

Fig. 8—The distribution of the solid α_1-Al phase solidified in the shot sleeve with a Gaussian distribution with a mean of 43.

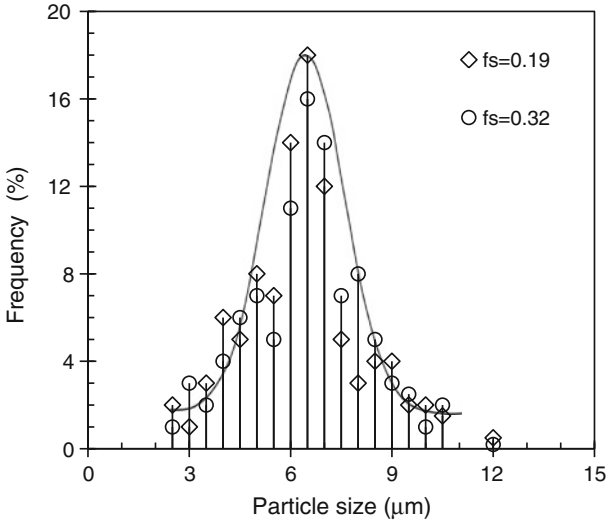

Fig. 9—The distribution of the solid α_2-Al phase solidified in the die cavity with a Gaussian distribution with a mean of 7.5.

It needs to be noted that the above stability equation was derived from the basic heat flow where consideration of the effect of the solute was not taken into account. However, Mullins and Sekerka[23] indicated that the stability criterion for diffusion-controlled growth of a sphere of fixed composition in a supersaturated solution is completely analogous to that of Eq. [1] if no heat flows inside the sphere.[24] In addition, the velocity at the interface calculated from heat flow considerations equals that calculated from mass diffusion considerations at local interface equilibrium.[24] When considering the instability problem of a growing interface in an alloy melt, for instability to occur, constitutional supercooling must exceed a specified value.[25,26] Then Eq. [1] is applicable to the spherical growth of a crystal in a supercooled multicomponent alloy.

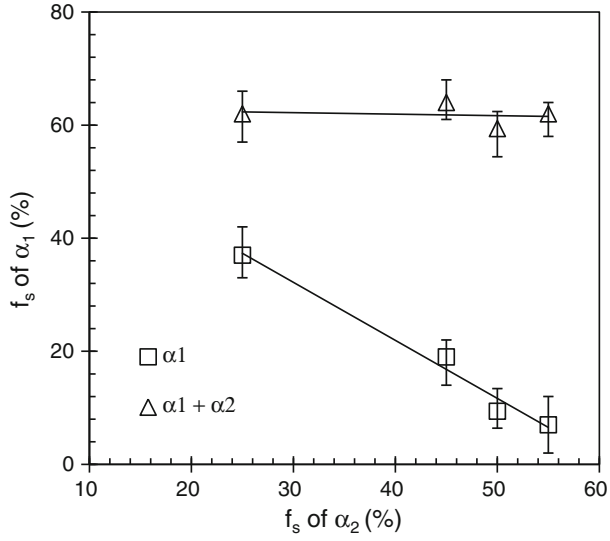

Fig. 10—The relationship between the solid fraction of the α-Al phase solidified in the shot sleeve (α_1) and that solidified in the die cavity (α_2).

According to this stability criterion for spherical growth in a uniformly supercooled melt, one can predict that all solid spheres undergoing thermally controlled growth are morphologically stable by substituting respective values in Table I[27,28] for k_l, k_s, γ_{SL}, L_v, and T_m into Eq. [1] giving

$$R_c = \frac{5.12}{\Delta T} \qquad [2]$$

Owing to the unavailability of some thermal and physical properties for the particular Al-5Mg-1.5Si-0.6Mn-0.2Ti alloy in the current study, the relevant data of pure Al were used in the calculation of Eq. [1]. As shown in Figure 16, the calculation indicates that the critical radius for spherical growth of aluminum crystal, R_c, is quite sensitive to the undercooling for spherical growth. For example, when ΔT = 1 K, all spherical aluminum crystals less than 10.24 μm in size will be stable for spherical growth. By contrast, when ΔT = 0.1 K, all grains smaller than 102.4 μm will be spherically stable. It is obvious that a smaller undercooling will promote the formation of larger spherical crystals during solidification.

For Al-based alloy, Burden and Hunt[29,30] measured the undercooling of an Al-Cu alloy. They found that the undercooling temperature was 1 through 2 K in the growth velocity ranging from 1 to 300 μm/s, and the temperature gradient was <10 K/cm during solidification of Al-2 wt pct Cu alloy. As it is understandably difficult to directly measure the undercooling in the die-casting process, we need to postulate the undercooling in the die cavity on the basis of the similarity of the physical properties during solidification of Al-Cu and Al-Mg alloys.[31] If we assume undercooling is at a similar level of 1 through 2 K during solidification in the die cavity, the stable spherical growth of α-Al crystals will range between 5.12 and 10.24 μm in diameter

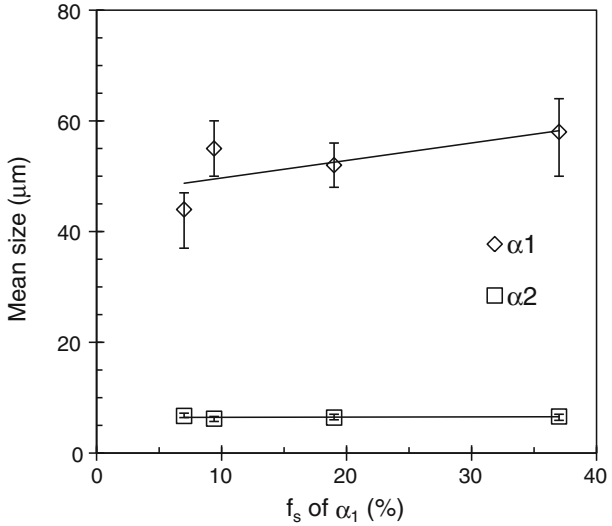

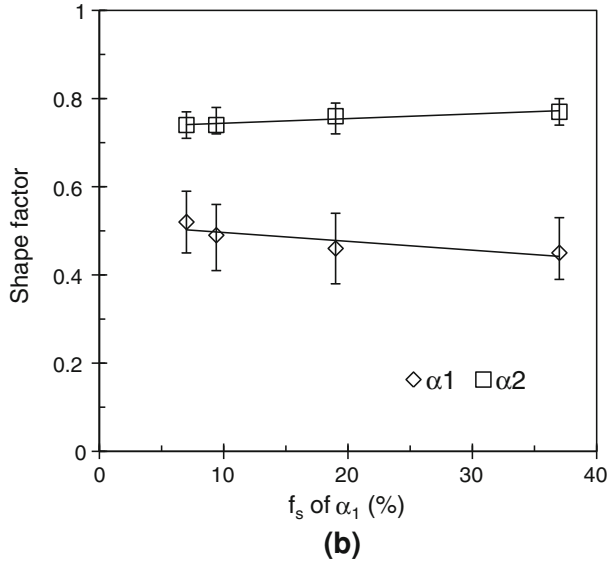

Fig. 11—The mean size (*a*) and the shape factor (*b*) of the primary α-Al phase solidified in the shot sleeve (α_1) and in the die cavity (α_2) as a function of the solid fraction of α_1.

according to Mullins–Sekerka stability theory. In fact, the measured α-Al grain size is 7.5 μm formed in the die cavity, indicating that the α-Al grain is close to its spherical growth limit. The microstructures also show large grains with a perturbed periphery. These might be over the critical size and have just lost their spherical morphology. This can be further examined according to similar experimental results. Bower *et al.*[32] have shown that the secondary dendrite arm spacing DAS varies approximately as the cube root of the local solidification time over a wide range of solidification conditions for Al-4.5 wt pct Cu alloy. We can, therefore, approximately estimate the local solidification time for the α-Al in the AlMgSi alloy. As the average grain size has been measured to be 7.5 μm, it gives a local solidification time of about 1s according to the measurement results in Reference 32. This gives a growth rate of 3.9 μm/s.

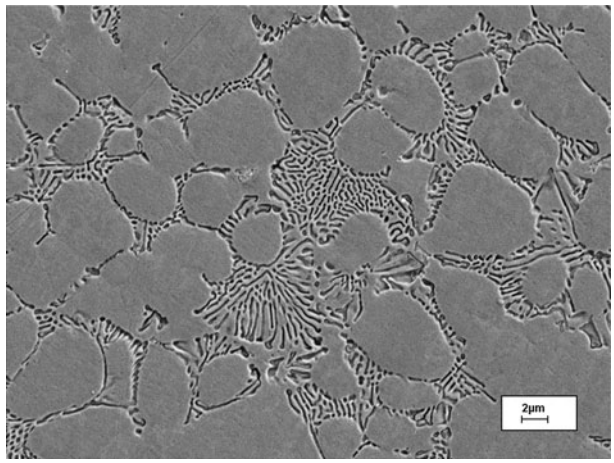

Fig. 12—SEM micrograph showing the structure of fine α_2-Al phase solidified inside the die cavity. The boundaries of the α_2-Al phase are well defined by the grain boundaries and the eutectic phase.

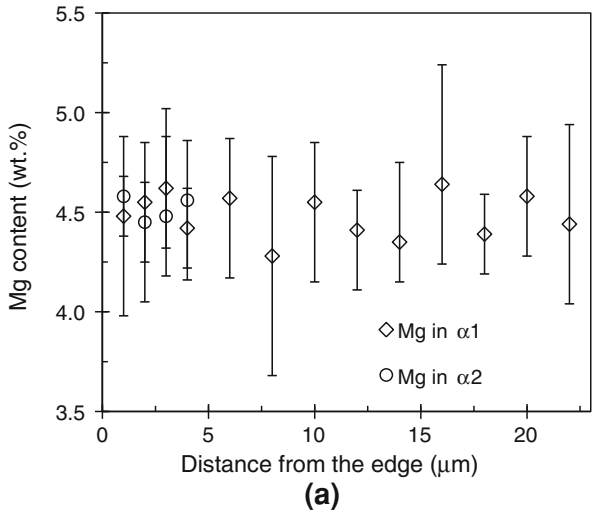

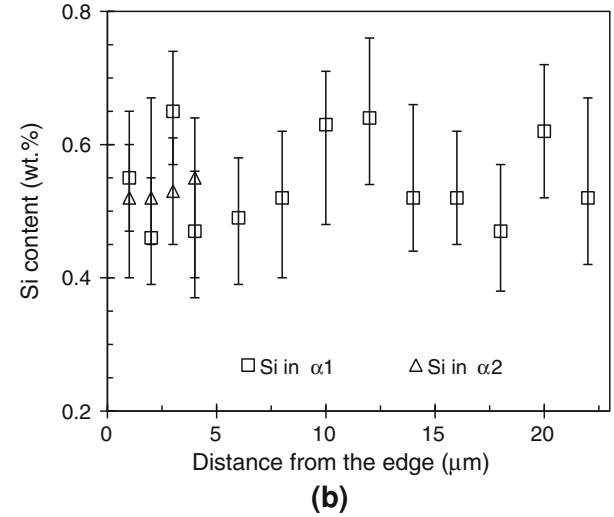

Fig. 13—SEM/EDS results showing (*a*) the solid solubility of Mg and (*b*) the solid solubility of Si in the primary α-Al phase solidified in the die cavity (α_2), and in the shot sleeve (α_1).

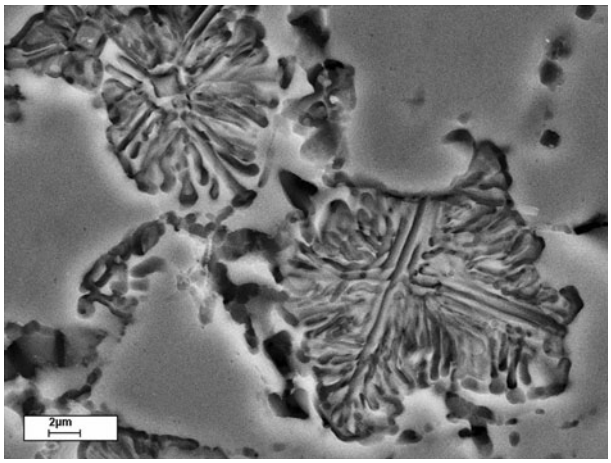

Fig. 14—SEM micrograph, taken from a deep-etched Al-5 wt pct Mg-1.5 wt pct Si-0.6 wt pct Mn-0.2 wt pct Ti diecast specimen, showing the morphology of the fine lamellar eutectic phase.

According to Burden and Hunt,[29,30] an undercooling is expected to be 1.3 K at this growth rate. The Mullins–Sekerka critical value can then be calculated at 7.9 μm, which is close to but larger than the average size measured in this study. As a result, grain growth during solidification within the die cavity can be within the stable growth regime and form a globular microstructure. It needs to be noted that the growth of primary α-Al grains may be altered when the processing conditions change during solidification. For example, when the cooling rate decreases and the wall thickness of the casting increases, the undercooling becomes smaller and thus promotes the formation of larger spherical grains and vice versa. It needs to emphasize that the growth velocities of the primary aluminum grains described above is speculative on the basis of previous experimental results. Therefore, the calculated results may not be very accurate. The grains could have stopped growing as primary phase because of the occurrence of eutectic solidification at the given time. However, the results provide good indication to understand the solidification process in HPDC.

The results from Mullins–Sekerka growth theory can also be used to explain the formation of the dendritic α-Al phase formed in the shot sleeve (α_1). The melt usually stays in the shot sleeve for 2 through 3 seconds from the time of pouring into the shot sleeve to the time of injection through the ingate of the casting. If it is assumed that a similar growth velocity of 3.9 μm/s exists for the α-Al phase, then the resultant spherical growth of the primary α-Al grains is 23.4 μm. In fact, the growth rate is smaller than 3.9 μm/s because the solidification in the shot sleeve is similar to gravity die casting with relatively lower cooling rates. Therefore, the resultant spherical growth of the primary α-Al grains formed in the shot sleeve is less than 23.4 μm. However, the measured size of the primary α-Al phase is 43 μm, which is much larger than the critical size predicted by the Mullins–Sekerka theory. Therefore, the grains will lose their stability for spherical growth and form a dendritic morphology.

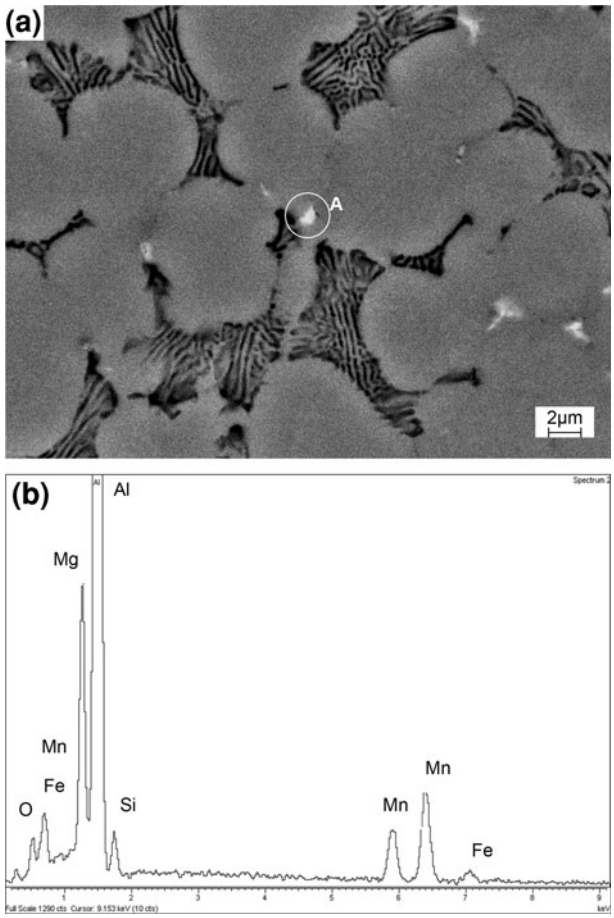

Fig. 15—(*a*) Backscattered SEM micrograph showing the distribution of intermetallics along grain boundaries in Al-5 wt pct Mg-1.5 wt pct Si-0.6 wt pct Mn-0.2 wt pct Ti diecast alloy, and (*b*) EDS spectrum showing the elements in particle A include Al, Mn, Si, and Fe.

B. *Formation of the Eutectic Phase*

The formation of the intergranular eutectic Mg_2Si phase between the α-Al phase marks the completion of solidification in the HPDC process. The faceted Mg_2Si phase can have a diversity of morphologies such as rod-like, crossed and rooftop-like, which has the same preferred [100] growth direction.[33] In the current study, the formation of fine eutectic Al-Mg_2Si lamellae is attributed to the high local cooling rate. Because the solidification inside the die cavity includes the evolution of primary α-Al grains that may divide the remnant liquid into very small pockets in between. Therefore, the eutectic reaction is confined to the small intergranular areas. The high local cooling rate is then able to contribute to the formation of the fine eutectic morphology. According to the equilibrium Al-Mg-Si phase diagram,[21] the formation of the eutectic Al-Mg_2Si phase is at a temperature close to 868 K (595 °C) when Mg is 5 wt pct. This is higher than the eutectic temperature of Al-Mg binary alloy at 725 K (451 °C). This confirms that the addition of Si into Al-Mg alloy reduces the solidification range and is beneficial for die casting which requires a narrow solidification range.[34]

Table I. Thermochemical and Physical Properties of Solid and Liquid Aluminum at Melting Point

Name	Symbol	Unit	Value	References
Melting Point	T_m	K	933.5	[27]
Density of Liquid Aluminum at T_m	ρ_L	g/cm^3	2.385	[27]
Volume Change from Solid to Liquid at T_m	ΔV_m		6.5 pct	[27]
Density of Solid Aluminum at T_m	ρ_S	g/cm^3	2.540*	
Thermal Conductivity of Liquid Aluminum at T_m	k_L	W/m/K	94.03	[27]
Thermal Conductivity of Solid Aluminum at T_m	k_S	W/m/K	238**	
Latent Heat of Fusion Per Mole of Aluminum	L_m	J/mol	1.047×10^4	[27]
Latent Heat of Fusion Per Unit Volume of Aluminum	L_v	J/m^3	$9.857 \times 10^{8\dagger}$	[27]
Solid–Liquid Interfacial Free Energy of Aluminum at T_m	γ_{SL}	J/m^2	158×10^{-3}	[28]

*Calculated according to ΔV_m and ρ_L at melting point T_m.
**The value of k_s is not available. The value given here is for 673 K (400 °C).
†Calculated from L_m/k_s.

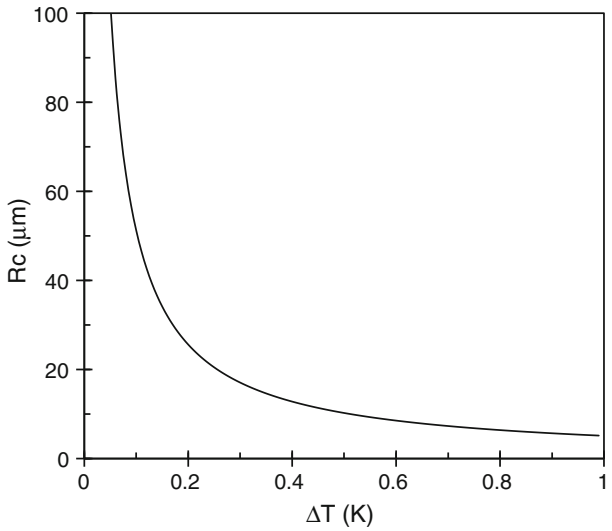

Fig. 16—The critical radius R_c for the spherical growth of aluminum crystals as a function of undercooling according to the Mullins–Sekerka growth theory.[23]

The direct measurement of the as-cast samples shows that the average eutectic spacing λ of the eutectic α-Al phase is 0.41 μm in the AlMgSi alloy. According to the Jackson–Hunt theory of eutectic growth,[35] the relationship between eutectic spacing λ and growth velocity V is as follows:

$$\lambda^2 V = \text{constant} \qquad [3]$$

Although the Jackson–Hunt theory is generally suitable for most eutectic reactions, the determination of the constant is still a challenge, and the results vary from one to another. The constant was measured to be $\lambda\sqrt{V} = 25.2 \pm 3.2$ $\mu m^{3/2}s^{-1/2}$ by Grugel and Kurz[36] for Al-Si alloys with 6 through 12 wt pct Si. The measurement carried out by Böyük *et al.*[37] for Al-11.1 wt pct Si-4.2 wt pct Ni eutectic alloy gave the dependency of λ_{Si} and λ_{Al_3Ni} on the values of V to be $\lambda_{Si} = 12.58V^{-0.50}$, $\lambda_{Al_3Ni} = 7.94V^{-0.47}$. The $\lambda^2 V$ value equals to 30.609 μm^3/s obtained by Kaya[38] and 19.6 μm^3/s by Whelan and Haworth[39] for Bi-Cd eutectics, but equals to 21.1 μm^3/s by Trivedi *et al.*,[40] 21.8 μm^3/s by Moore and Elliot,[41] and 23.7 μm^3/s by Cadirli *et al.*[42] for Pb-Cd eutectic system. Kaya *et al.*[37] obtained $\lambda^2 V = 39.059$ μm^3/s for Al-Cu eutectic, while Cadirli *et al.*[43] provided a value of 156 μm^3/s for a similar alloy.

Because of the lack of data for the AlMgSi alloy, we could take the constant for a range of 15 to 30 μm^3/s to get an approximate solution. If $\lambda^2 V$ = 15 to 30 μm^3/s, as λ is measured at 0.41 μm, we can have $V = 89$ to 178 μm/s. This means that very fast solidification has occurred in the die cavity during solidification. However, the growth rate calculated for the eutectic phase is much larger than that of the primary α-Al phase. This can be attributed to the estimation of the constant. If we calculate the constant in Eq. [3] by using the growth rate of 3.9 μm/s obtained from the primary α-Al phase, then $\lambda^2 V$ is 0.656 μm^3/s. This constant is smaller than the data reported in References 37 through 43. It has to be pointed out that the constant $\lambda^2 V$ for a specific eutectic was usually obtained under controlled and constrained conditions, *e.g.*, by directional growth, and that for the eutectic growing into an undercooled melts the Jackson–Hunt model might not be valid, *i.e.*, $\lambda^2 V$ might not be constant anymore. It is true that, as indicated by the TMK model,[44,45] the $\lambda^2 V$ is deviated from a constant value when the undercooling is very large and growth rate is very high. In the current study, however, this deviation is believed not to be very much because the growth rate and undercooling during a HPDC process are still low enough compared with the cases analyzed in the TMK model.[44,45] It is therefore observed that the approximately estimated growth velocity from the Jackson–Hunt model here is reasonable.

C. *Formation of the Intermetallics*

Iron is unavoidably picked up in HPDC process and is also a useful minor alloying element in aluminum alloys to facilitate ejection and to help die-release.[46] However, the presence of excessive Fe is significantly detrimental to the ductility because of its low equilibrium solubility in the α-Al solid solution phase (<0.04 wt pct).[47] Although a wide range of iron-rich compounds

have been reported in the literature,[48,49] they can generally be divided into three different morphologies: polyhedral crystals, Chinese script, and thin platelets. Addition of Mn into aluminum alloys can modify the morphology and the type of the Fe-rich intermetallic phases from platelets to a more cubic form or to globules.[50,51] According to Mondolfo,[52] $Al_6(FeMn)$ is the first phase to form in Al-Fe-Mn-Si system, and then $Al_6(FeMn)$ reacts peritectically with the liquid to form the compact $Al_{15}(FeMn)_3Si_2$. All the Mn-containing compounds have more or less equiaxed crystal structures and tend to solidify in a compact morphology. In general, the manganese content should not be less than half of the iron content for commercial aluminum alloys that contain iron exceeding 0.45 wt pct.[53]

In the current study, Mn is added at a level of 0.6 wt pct, which is sufficiently high compared with the iron content. Therefore, the formation of Al_3Fe, Al_8Fe_2Si, or Al_5FeSi phases can be prevented during solidification. As a result, the compact α-AlFeMnSi phase is the main intermetallic compound in the alloy, minimizing the detrimental effect of intermetallics on the mechanical properties, especially the ductility of the alloy.

V. CONCLUSIONS

1. In the HPDC of ductile aluminum alloys, solidification commences with the formation of primary α-Al phase in the shot sleeve and is completed in the die cavity. The primary α-Al phase formed in the shot sleeve is characterized by the dendrites and fragmented dendrites with the size ranging from 15 to 100 μm and an average of 43 μm. The primary α-Al phase formed in the die cavity is characterized by fine globular grains with an average of 7.5 μm in size. Solidification inside the die cavity is also responsible for the formation of the lamellar Al-Mg_2Si eutectic and the Fe-rich intermetallic. The size of the eutectic cells is about 10 μm, in which the lamellar α-Al phase is 0.41 μm in thickness.
2. The intermetallic compounds exhibit a compact morphology with a size smaller than 2 μm and are located at the boundaries between the primary α-Al grains or between eutectic cells and the primary α-Al grains. The intermetallic contains 1.62 at. pct Si, 3.94 at. pct Fe, and 2.31 at. pct Mn, suggesting that it is most likely the α-AlFeMnSi phase.
3. A solute-enriched circular band is always observed parallel to the surface of the casting. The band zone separates the outer skin from the central region of the casting. The solute concentration is consistent in the skin region and a general drop toward the center inside the band for Mg and Si. The peak of solute enrichment in the band zone is much higher than the nominal composition of the alloy. However, the die casting exhibits a combination of brittle and ductile fracture. There is no significant difference on the fracture morphology in the three regions. Therefore, the band zone is not significantly detrimental in terms of the fracture mechanism in the die casting.
4. The stability criterion developed by Mullins and Sekerka for spherical growth can be used to provide a reasonable explanation for the difference in morphology of the primary α-Al phase solidified in the shot sleeve and in the die cavity. The solidification of the α-Al phase inside the die cavity has been completed before the spherical grains begin to lose their stability, but the grains in the shot sleeve exceed the limit of spherical growth and, therefore, exhibit a dendritic morphology.
5. The Jackson–Hunt theory can be used to estimate the growth rate of eutectic Al-Mg_2Si phase in HPDC process, and the results indicate that a fast solidification rate occurs in the die cavity. However, the growth rate of the aluminum phase in eutectic solidification calculated using the Jackson–Hunt theory is much larger than the growth rate of the primary α-Al phase calculated using the Mullins and Sekerka theory.

ACKNOWLEDGMENTS

The authors wish to thank EPSRC and JLR for the financial support.

REFERENCES

1. E.J. Vinarcik: *High Integrity Die Casting Processes*, Wiley, New York, 2003.
2. H.L. MacLean and L.B. Lave: *Prog. Energy Combust. Sci.*, 2003, vol. 29 (1), pp. 1–69.
3. W.S. Miller, L. Zhuang, J. Bottema, A.J. Wittebrood, P. DeSmet, A. Haszler, and A. Vieregge: *Mater. Sci. Eng. A*, 2000, vol. A280 (1), pp. 37–49.
4. R.J. Orsato and P. Wells: *J. Cleaner Prod.*, 2007, vol. 15 (11–12), pp. 994–1006.
5. J.T. Staley and D.J. Lege: *J. De Physique IV*, 1993, vol. 3, pp. 179–90.
6. A. Tharumarajah: *Resour. Conserv. Recycl.*, 2008, vol. 52, pp. 1185–89.
7. D. Carle and G. Blount: *Mater. Des.*, 1999, vol. 20 (5), pp. 267–72.
8. European Aluminium Association: *Aluminium in Cars*, European Aluminium Association, 2008.
9. S. Ji, D. Watson, Z. Fan, and M. White: *Mater. Sci. Eng. A*, 2012, vol. 556, pp. 824–33.
10. D. Apelian: *Aluminium Cast Alloys: Enabling Tools for Improved Performance*, North American Die Casting Association, Wheeling, IL, 2009, pp. 1–68.
11. P. Krug, H. Koch, and R. Klos: Magsimal-25—A new High-Ductility Die Casting Alloy for Structural Parts in Automotive Industry, www.dgm.de/download/tg/523/523_0784.pdf.
12. M. Hosseinifar and D.V. Malakhov: *Metall. Mater. Trans. A*, 2011, vol. 42A, pp. 825–33.
13. Y.L. Liu and S.B. Kang: *J. Mater. Sci.*, 1997, vol. 32, pp. 1443–47.
14. S.A. Kori, M.S. Prabhudev, and T.M. Chandrashekharaiah: *Trans. Indian Inst. Met.*, 2009, vol. 62, pp. 353–56.
15. L. Yu, X. Liu, Z. Wang, and X. Bian: *J. Mater. Sci.*, 2005, vol. 40, pp. 3865–71.
16. S. Otarawanna, C.M. Gourlay, H.I. Laukli, and A.K. Dahle: *Metall. Mater. Trans. A*, 2009, vol. 40A, pp. 1645–59.
17. J. Jie, C. Zou, H. Wang, and Z. Wei: *Mater. Lett.*, 2010, vol. 64, pp. 869–71.
18. R. Kimura, H. Hatayama, K. Shinozaki, I. Murashima, J. Asada, and M. Yoshida: *J. Mater. Process. Technol.*, 2009, vol. 209 (1), pp. 210–15.

19. A. Hamasaiid, M.S. Dargusch, C.J. Davidson, S. Tovar, T. Loulou, F. Rezai-Aria, and G. Dour: *Metall. Mater. Trans. A*, 2007, vol. 38A, pp. 1303–15.
20. A.K. Dahle and D.H. StJohn: *Acta Mater.*, 1999, vol. 47, pp. 31–41.
21. V. Raghavan: *J. Phase Equilib. Diffus.*, 2007, vol. 28, pp. 189–91.
22. P. Beeley: *Foundry Technology*, 2nd ed., Butterworth-Heinemann, Oxford, 2001.
23. W.W. Mullins and R.F. Sekerka: *J. Appl. Phys.*, 1963, vol. 34, pp. 323–29.
24. W.W. Mullins and R.F. Sekerka: *J. Appl. Phys.*, 1964, vol. 35, pp. 444–51.
25. R.F. Sekerka: *J. Appl. Phys.*, 1965, vol. 36, pp. 264–68.
26. D.P. Woodruff: *The Solid–Liquid Interface*, Cambridge University Press, Cambridge, 1973.
27. E.A. Brandes and G.B. Brook: *Smithells Metals Reference Book*, 7th ed., Butterworth, Oxford, 1992.
28. A.L. Greer, A.M. Bunn, A. Tronche, P.V. Evans, and D.J. Bristow: *Acta Mater.*, 2000, vol. 48, pp. 2823–35.
29. M.H. Burden and J.D. Hunt: *J. Cryst. Growth*, 1974, vol. 22, pp. 99–108.
30. J.D. Hunt and S.Z. Lu: *Metall. Mater. Trans. A*, 1996, vol. 27A, pp. 611–23.
31. K. Keslioglu, M. Gunduz, H. Kaya, and E. Cadırl: *Mater. Lett.*, 2004, vol. 58, pp. 3067–71.
32. T.F. Bower, H.D. Brody, and M.C. Flemings: *Trans. AIME.*, 1966, vol. 236, pp. 624–33.
33. S.-P. Li, S.-X. Zhao, M.-X. Pan, D.-Q. Zhao, X.-C. Chen, and O.M. Barabash: *J. Mater. Sci.*, 2001, vol. 36, pp. 1569–75.
34. J Cambell: *Castings*, 2nd ed., Elsevier Butterworth-Heinemann, Oxford, 2003.
35. K.A. Jackson and J.D. Hunt: *Trans. Metall. Soc. AIME.*, 1966, vol. 236, pp. 1129–42.
36. R. Grugel and W. Kurz: *Metall. Trans. A*, 1987, vol. 18, pp. 1137–42.
37. U. Böyüka, S. Enginb, and N. Maraşlı: *Mater. Charact.*, 2011, vol. 62 (9), pp. 844–51.
38. H. Kaya, E. Cadirli, and M. Gündüz: *J. Mater. Process. Technol.*, 2007, vol. 183 (2–3), pp. 310–20.
39. E.P. Whelan and C.W. Haworth: *J. Aust. Inst. Met.*, 1967, vol. 12, pp. 77–126.
40. R. Trivedi, J.T. Mason, J.D. Verhoeven, and W. Kurz: *Metall. Trans. A*, 1991, vol. 22A, pp. 2523–33.
41. A. Moore and R. Elliott: in *Proc. Conf. Iron and Steel*, Ins. Publ., Brighton, 1967, pp. 167–74.
42. E. Cadirli, H. Kaya, and M. Gunduz: *Mater. Res. Bull.*, 2003, vol. 38, pp. 1457–76.
43. E. Cadirli, A. Ulgen, and M. Gunduz: *Mater. Trans. JIM*, 1999, vol. 40, pp. 989–96.
44. R. Trivedi, P. Magnin, and W. Kurz: *Acta Metall.*, 1987, vol. 35, pp. 971–80.
45. W. Kurz and R. Trivedi: *Metall. Trans. A*, 1991, vol. 22A, pp. 3051–57.
46. L. Wang, M. Makhlouf, and D. Apelian: *Int. Mater. Rev.*, 1995, vol. 40, pp. 221–38.
47. L.F. Mondolfo: *Aluminium Alloys: Structure and Properties*, Butterworths, London, 1976.
48. S.G. Shabestari: *Mater. Sci. Eng. A*, 2004, vol. 383A, pp. 289–300.
49. G. Gustafsson, T. Thorvaldsson, and G.L. Dunlop: *Metall. Trans. A*, 1986, vol. 17A, pp. 45–52.
50. S.G. Shabestari, M. Mahmudi, M. Emami, and J. Campbell: *Int. J. Cast Met. Res.*, 2002, vol. 15, pp. 17–24.
51. J.L. Jorstad: *Die Casting Eng.*, 1986, vol. 11/12, pp. 23–27.
52. L.F. Mondolfo: *Manganese in Aluminium Alloys*, The Manganese Centre, Paris, 1978.
53. A. Couture: *A.F.S. Int. Cast Met. J.*, 1981, vol. 6 (4), pp. 9–17.